Ethylene Carbonate−Li^+: A Theoretical Study of Structural and Vibrational Properties in Gas and Liquid Phases

Marco Masia,*,† Michael Probst,‡ and Rossend Rey†

Departament de Física i Enginyeria Nuclear, Universitat Politècnica de Catalunya, Campus Nord B4-B5, Barcelona 08034, Spain, and Institute of Ion Physics, Universität Innsbruck, Technikerstrasse 25, Innsbruck A-6020, Austria

Received: September 8, 2003; In Final Form: December 5, 2003

Structural and dynamical properties of the electrolyte system ethylene carbonate−Li^+ are studied. A high-level ab initio study of the geometry and vibrational spectrum has been performed both for an isolated molecule and for small clusters including the lithium ion. The ethylene molecule is found to be nonplanar in all instances, and an assignment of vibrational modes is proposed on this basis. It is shown that the lithium ion induces substantial blue- and redshifts, mainly on the ring- and carbonyl-stretching modes. These issues have also been studied in the liquid phase for the first time, and for that purpose, a new intramolecular force field has been developed. It is shown that this intramolecular potential satisfactorily reproduces a broad range of features, allowing us to interpret the shifts measured experimentally for the molecules within the first solvation shell of the ion. Particularly, the broadening of the carbonyl band found experimentally is the result of an ion-induced redshift, obscured by the presence of Fermi resonances. Moreover, the study of the shifts as a function of solvation number supports a 4-coordinated solvation shell.

I. Introduction

In recent years, ethylene carbonate has been the subject of an increasing interest due to its important role in polymer−gel lithium-ion batteries.[1] These devices are usually composed of a lithium salt dissolved in a plasticizer (i.e., an organic solvent) that fills a polymer matrix. Some common solvents are ethylene carbonate (EC, see Figure 1), tetrahydrofuran, propylene carbonate (PC), and γ-butyrolactone.[1] Actually, a mixture of two or more plasticizers is more convenient,[2] as it allows us to optimize the balance between different features (such as dielectric constant, viscosity, ionic diffusion, salt dissociation, and chemical stability) and thus to enhance the battery performace and cyclability. Understanding the molecular mechanisms by which these plasticizers condition the mobility of lithium is, therefore, of particular interest. Conversely, the strong influence of the ion can substantially affect the surrounding solvent molecules, particularly in their structure and vibrational spectrum. These properties, which can be experimentally probed by a variety of mostly spectroscopical methods, are also amenable to a direct computational study. The motivation of the present work is that a better theoretical understanding of these solvation properties is not only of interest in itself but also a convenient benchmark for the models that will be used to address the basic problem of lithium mobility.

Concerning the structure of the EC molecule, early experimental results of Angell[3] pointed to a planar configuration; later Wang et al.,[4] Fortunato et al.,[5] Alonso et al.,[6,7] and Matias et al.[8] found that EC has a nonplanar ring structure. On the theoretical side, the structural problem has received much attention as well, with the results alternating between both possibilities, the initial computations supported a nonplanar structure,[7,9] subsequent works were in favor of a planar configuration,[10−12] while the most recent results favor again a distorted configuration.[13−15] Regarding the vibrational spectrum, many IR and Raman studies have been performed of pure EC and of lithium salts dissolved in liquid EC.[5,11,16−20] From the theoretical point of view, the vibrational spectrum has barely

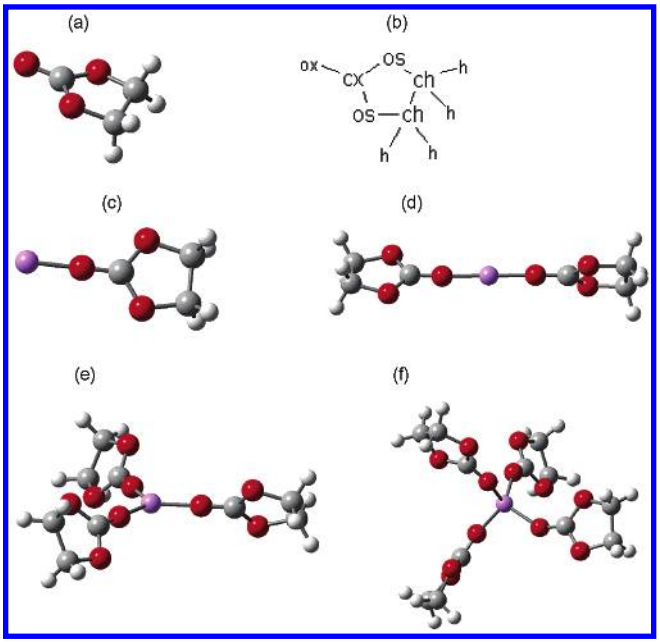

Figure 1. Ethylene carbonate and its complexes $[Li(EC)_n]^+$ with $1 \leq n \leq 4$. The labeling of the atoms used in the text is defined in (b). The following colors are assigned to different atomic species: red to oxygen, gray to carbon, white to hydrogen, and violet to lithium. Bonds connecting lithium to carbonyl oxygens are included as a guide to the eye.

* Author to whom correspondence may be addressed. E-mail: marco.masia@upc.es.
† Universitat Politècnica de Catalunya.
‡ Universität Innsbruck.

10.1021/jp036673w CCC: $27.50
Published on Web 01/16/2004

been addressed, we only know of the ab initio study of Klassen et al.[11] for gas-phase EC. For this reason, it will be the main aim of this work to study the dependence of the vibrational modes on geometry and complexation of EC.

We address several issues with both first-principles calculations and classical molecular dynamics simulations (MD). First, we have performed the highest-level ab initio study to date of the single EC molecule, determining which is the most stable geometry and analyzing the issue of band assignment. Of particular interest to MD simulations of the liquid, a new intramolecular force field is developed (in terms of valence coordinates) that represents quite satisfactorily not only the vibrational spectrum but also several other aspects of the full internal potential (particularly the barriers to internal isomerization in the low-frequency region, relevant to liquid-state dynamics). Moreover, the series of clusters $[Li(EC)_n]^+$ ($n = 1-4$) has also been addressed by analyzing the equilibrium geometries and the molecular vibrations in detail. These complexes constitute a useful guide to ascertain which are the EC modes most affected by the ion and how this effect (and the possible ion-induced geometry distortion) varies as the coordination is increased, which should help understand the liquid-state results. In this connection, MD simulations of the liquid phase have been done for pure EC and for one lithium ion dissolved in liquid EC, focusing on the theoretical calculation of the frequency shifts induced on the first-shell molecules surrounding the ion. Finally, an analysis of the most probable configurations has also been performed, complementing the MD studies of coordination shell structure by Li et al.[12] and Soetens at al.[13,21]

The paper is organized as follows: computational details are summarized in section 2; results from ab initio calculations are discussed in section 3; and those from classical simulations are discussed in section 4. Finally, the main conclusions are presented in section 5.

II. Computational Details

All ab initio calculations were performed using the commercial package Gaussian 98.[22] Vibrational analysis and geometry optimization of a single EC molecule and of the complex $[LiEC]^+$ were performed at the MP2 level with the 6-311G basis set augmented with diffuse and polarization functions.[23] The same model chemistry has been employed for a potential-energy surface scan of EC. We also performed a geometry optimization for the single EC molecule using Dunning's correlation-consistent basis set, including polarization and diffuse functions aug-cc-pVDZ. As far as we know, this is the highest-level geometry optimization of EC appearing in the literature, providing results in very good agreement with experiment. The additional calculations with the 6-311++G(d,p) basis set were performed to allow for a better comparison between the EC monomer and the $[LiEC]^+$ dimer since the aug-cc-pVDZ basis set is not defined for lithium. Because of the demanding computational effort of ab initio calculations on the systems with up to four EC molecules, a smaller basis set (6-31G) was used for their geometry optimizations and vibrational analysis.

Classical calculations were performed with both our own molecular mechanics code and with the DL_POLY[24,25] set of programs. The first one was used for the scan of the potential-energy surface of a single EC molecule using an internal classical force field and for the vibrational analysis of EC. The DL_POLY package was used to perform the simulations of the chosen liquid-phase systems. Data analysis (FFT, curve smoothing, and curve fitting) was performed with the commercial package Microcal Origin 6.1.[26]

III. Ab Initio Results

A. Structure. *1. Single EC Molecule.* As previuosly described, the equilibrium geometry of an EC molecule is a topic that has received considerable experimental and theoretical attention over the years.

To our knowledge, the only experiment where a planar structure has been inferred was performed by Angell[3], who observed the disappearance of some spectral lines in passing from solid to liquid and gas phases and attributed this to the enhanced symmetry when the molecule passes from C_2 to C_{2v}. Planarity is contradicted by more recent microwave measures,[4] where the appearance of doublets of similar intensity for rotational transitions is explained assuming a nonplanar ground-state tunneling through the barrier at the planar configuration. A nonplanar structure was also found by Alonso at al.[6,7] with microwave spectroscopy and by Matias et al.[8] in a neutron-diffraction study.

Surprisingly, rather recent theoretical results support different structures. Blint[10] points out that the structure of pure EC is planar and that the barrier to reach a distorted configuration is $\sim$15 kcal mol^{-1}, making use of a HF/D95V** model chemistry; the same results were obtained by Klassen et al.[11] with the same model chemistry and by Li et al.,[12] who made use of a DFT optimized geometry. These findings contradict the expectation of Cremer and Pople who, in their study on general monocyclic rings,[27] claimed that a twisted conformation is preferred because a planar ring would imply a more highly strained ring angle at the carbonyl atom. Indeed, in a pioneering study, Alonso et al.[6] found that a double well potential for the ring puckering exists, with two minima different from zero; they argued that this is due to the sum of two opposing contributions where the one that causes the ring to be twisted dominates on the second that would lead to a planar structure; to get a proper description of the molecule, they suggest the use of a rather flexible orbital basis. It is possible that previous studies[10−12] did not find these results because their methods underestimate electron correlation. The nonplanarity of the ring has been recently found with higher-level ab initio calculations by Soetens et al.[13] and Wang et al.[14]

From the geometry optimization of EC, we have also found that the ring shows a nonplanar structure with C_2 symmetry. Table 1 contains the values for the internal coordinates (at MP2/aug-cc-pVDZ and MP2/6-311++G(d,p) levels of theory) and the values inferred experimentally for pure EC.[8] It can be seen that there is good agreement between theory and experiment, mainly at the higher-level calculations. Concerning the extent of ring distortion, panel c of Figure 3 displays the double-well symmetric potential from an optimized relaxed potential-energy surface (rPES) scan of the os-ch-ch-os dihedral angle (see Figure 1 for the labeling of atoms within the EC molecule). A rPES scan computes the energy along a given internal coordinate, simultaneously optimizing all the unconstrained internal degrees of freedom at each step (the Berny geometry optimization algorithm[28] with redundant internal coordinates[29] is used). For this particular coordinate, 60 values of the dihedral angle within -50 and 50° were scanned using an MP2/6-311++G(d,p) model chemistry for the geometry optimization. We find an energy barrier for ring inversion of $\sim$1.30 kcal mol^{-1}. The equilibrium value is $\sim-29°$ ($\sim$0.78 kcal mol^{-1} at $\sim-27°$ were obtained with the aug-cc-pVDZ basis set). Our values are slightly higher than previous estimations for both the equilibrium

TABLE 1: Comparison of Experimental and Theoretical Geometrical Parameters for EC and for the Optimized Geometry of the EC−Li^+ Complex

	EC			$[Li(EC)]^+$
	exp	aug-cc-pVDZ	6-311++G(d,p)	6-311++G(d,p)
		Bond Length		
ox-cx	1.203	1.203	1.193	1.220
cx-os	1.342	1.370	1.360	1.320
os-ch	1.457	1.440	1.430	1.450
ch-ch	1.522	1.520	1.520	1.520
ch-h	1.091	1.090	1.080	1.080
		Bending Angle		
ox-cx-os	124.17	124.820	124.970	123.130
cx-os-ch	108.71	108.420	108.140	107.940
os-ch-ch	102.16	102.470	102.050	102.190
os-ch-h	108.30	108.300	108.600	107.552
os-cx-os	111.67	110.350	110.200	113.970
h-ch-h	110.82	110.513	110.610	111.140
ch-ch-h	113.94	114.000	114.030	113.190
		Dihedral Angle		
ox-cx-os-ch	-	170.550	169.760	171.650
cx-os-ch-ch	21.25	22.900	24.780	20.030
cx-os-ch-h	141.81	143.720	145.580	140.700
os-ch-ch-os	−24.80	−27.180	−29.410	−23.510
os-cx-os-ch	−8.73	−9.443	−10.269	−8.334
os-ch-ch-h	90.88	89.190	86.940	91.780
h-ch-ch-h	−154.32	−154.410	−156.650	−152.910
ox-cx-os-os	171.27	180.000	179.980	179.920

angle and barrier height. Alonso et al.[6,7] found a barrier height of ∼0.67 kcal mol^{-1} and an equilibrium angle of ∼−19° in the gas phase; Matias et al.[8] found a value of ∼−24.8° in the solid phase using neutron diffraction analysis. The most recent results, though, are rather similar to the ones obtained here; Soetens et al.[13] found an equilibrium dihedral of ∼29.5° and a barrier of 1.18 kcal mol^{-1} (using an MP2/6-311G** model chemistry). Finally, it is worth noting that the dipole moment of pure EC is 5.3945 D (5.4226 D was calculated with the 6-311++G(d,p) basis set). These values agree very well with experiment; Alonso et al.[6] report a value of 5.35 ± 0.15 D.

2. $[Li(EC)_n]^+$ (n = 1−4) Complexes. An interesting issue to look into is how a single EC molecule is affected when it coordinates the lithium ion and how this is changed by the addition of more molecules since such solvation properties are helpful in understanding the liquid solution. First, as found in previous works,[10,15] the optimized geometry (see Figure 1c) of all complexes studied is characterized by the lithium ion being close to the carbonyl oxygen. The last column of Table 1 contains the main structural properties of the monocoordinated lithium complex computed with a MP2/6-311++G(d,p) model chemistry. It is interesting to note that the coordination with Li^+ changes the EC conformation slightly toward a more planar geometry: the os-ch-ch-os dihedral angle reduces from 29.4 to 23.5° for a given level of theory (two last columns of Table 1). The induced distortion is also evident along other internal coordinates; the optimized carbonyl bond length increases from 1.193 Å in the isolated EC molecule to 1.220 Å in the complex. The ch-ch and the ch-h bond lengths do not seem to undergo any significant change as is easily explainable by the proximity of Li^+ to the carbonyl oxygen and its neighboring atoms.

In addition, we have also studied the effect of coordination in the complexes $[Li(EC)_n]^+$ with *n* varying from 1 to 4 (theoretical calculations suggest that the 4-coordinated complex is the one existing in condensed phase).[16,17] Because of computational limits, a smaller basis set (6-31G) was used for the geometry optimization of these complexes. Quantitative values at this level of theory are not sufficiently accurate but certain trends can nevertheless be predicted. As illustrated in Figure 1, all the complexes are found to be highly symmetrical; there is a linear arrangement for the complexes with one and two coordinating EC molecules. The 3-coordinated complex is trigonal planar with the ring forming an angle of ∼55° with the plane defined by lithium and the carbonyl oxygens. The 4-coordinated complex shows tetrahedral complexation. In the latter one, the EC dipole moment does not point straight to the ion, revealing that one of the two carbonate oxygens is nearer to the metal center. The shorter li-os distance is 3.630 Å, and the longer is 4.230 Å. This fact is confirmed by the value of the li-ox-cx angle, which changes from almost 180°(for the dimer) to 145°.

TABLE 2: Results of the Low-Level (MP2/6-31G) Geometry Optimization Results for the Structure of EC and Its Complexes with Lithium

	EC	$[Li(EC)]^+$	$[Li(EC)_2]^+$	$[Li(EC)_3]^+$	$[Li(EC)_4]^+$
		Bond Length			
li-ox		1.760	1.800	1.871	1.947
ox-cx	1.227	1.250	1.240	1.240	1.230
cx-os	1.410	1.360	1.370	1.380	1.380
os-ch	1.490	1.520	1.520	1.510	1.500
ch-ch	1.540	1.550	1.550	1.550	1.540
		Bending Angle			
li-ox-cx		179.98	178.00	179.86	145.32
ox-cx-os	125.36	123.26	123.66	123.99	124.11
os-cx-os	109.51	113.47	112.78	112.00	111.31
		Dihedral Angle			
ox-cx-os-ch	171.35	175.48	174.83	173.56	172.99
cx-os-ch-ch	21.44	11.14	13.14	15.96	17.93
os-ch-ch-os	−25.28	−12.89	−15.24	−18.59	−21.20
os-cx-os-ch	−8.63	−4.50	−5.35	−6.43	−7.76
ox-cx-os-os	179.95	180.00	179.88	180.00	179.88

Because of the symmetry in the complexes mentioned above, equilibrium values of the internal coordinates are equal for all coordinating EC molecules in each cluster. They are reported in Table 2. The most dramatic effect of coordination appears in the 1:1 complex where the os-ch-ch-os dihedral angle attains its lowest value and the ox-cx bond is maximally stretched. With increasing number of EC ligands, the li-ox distance increases and its geometry approaches the values of the isolated molecule. The ox-cx-os-os group preserves its planarity, as is expected for the carbonate fragment.

B. Vibrational Spectrum. *1. Single EC Molecule.* The first complete assignment of the vibrational frequencies of EC is that of Fortunato et al.[5] more than thirty years ago, based on the assumption of ring planarity and inferring the nature of the modes from experimental spectra. In accordance with the assumed geometry, the vibrational modes were classified in four symmetry species. More recently, this assignment has been revised by Klassen et al.[11] from ab initio calculations at the HF/D95V** level of theory although, again, a planar geometry is assumed. Considering the previously discussed growing theoretical and experimental evidence in favor of a nonplanar structure, it seems justified to revisit this issue and possibly renumber some of the vibrational modes. Table 3 contains the assignments proposed from the analysis of the present ab initio calculations (and in terms of the two symmetry species corresponding to a C_2 symmetry) together with Fortunato's assignment (this mapping should be useful when comparing future experimental and theoretical results with previous assignments). In the rest of this paper, we will stick to the new numbering given in the first column of Table 3. Concerning the dynamics associated with each mode, in most cases either the experimental assignments coincide with our ab initio results or the differences are minor; for example, ν_8 and ν_{19} are ring modes as indicated by Fortunato et al.,[5] but we specify which

TABLE 3: Computed Harmonic Frequencies for EC and Band Assignment Compared to the Experimental Frequencies and the Mode Assignment of Fortunato et al[5]

ν		assignment	exp		assignment
ν_1(a)	3194.2	out of phase CH_2 asym stretch	$\nu_9(a_2)$	3004	CH_2 stretching
ν_2(a)	3109.7	in phase CH_2 sym stretch	$\nu_1(a_1)$	2925	CH_2 stretching
ν_3(a)	1898.8	C═O stretching	$\nu_2(a_1)$	1868	C═O stretching
ν_4(a)	1546.8	in phase CH_2 scissoring	$\nu_3(a_1)$	1483	CH_2 scissoring
ν_5(a)	1420.0	out of phase CH_2 wagging	$\nu_4(a_1)$	1386	CH_2 wagging
ν_6(a)	1271.5	out of phase CH_2 twisting	$\nu_{10}(a_2)$	1157	CH_2 twisting
ν_7(a)	1175.2	**out of phase CH_2 rocking**[a]	$\nu_5(a_1)$	1087	**ring stretching**
ν_8(a)	1123.5	os-ch sym stretch, ch-ch stretch	$\nu_6(a_1)$	960	ring stretching
ν_9(a)	991.6	ring breathing	$\nu_7(a_1)$	881	ring breathing
ν_{10}(a)	895.3	**ring breathing**	$\nu_8(a_1)$	715	**ring bending**
ν_{11}(a)	719.6	**ring stretching**	$\nu_{11}(a_2)$	660	**CH_2 rocking**
ν_{12}(a)	227.2	**out of plane ring bending**	$\nu_{12}(a_2)$	230	**ring puckering**
ν_{13}(b)	3205.8	in phase CH_2 asym stretch	$\nu_{20}(b_2)$	3000	CH_2 stretching
ν_{14}(b)	3112.6	out of phase CH_2 sym stretch	$\nu_{13}(b_1)$	2925	CH_2 stretching
ν_{15}(b)	1539.4	out of phase CH_2 scissoring	$\nu_{14}(b_1)$	1483	CH_2 scissoring
ν_{16}(b)	1420.8	in phase CH_2 wagging	$\nu_{15}(b_1)$	1421	CH_2 wagging
ν_{17}(b)	1267.9	**in phase CH_2 twisting**	$\nu_{16}(b_1)$	1223	**ring stretching**
ν_{18}(b)	1138.4	**ring stretching**	$\nu_{21}(b_2)$	1218	**CH_2 twisting**
ν_{19}(b)	1079.2	os-ch asym stretch	$\nu_{17}(b_1)$	1125	ring stretching
ν_{20}(b)	919.0	in phase CH_2 rocking	$\nu_{22}(b_2)$	768	CH_2 rocking
ν_{21}(b)	779.7	out of plane ring C═O bending	$\nu_{18}(b_1)$	696	ring bending
ν_{22}(b)	673.4	**in plane ring distortion**	$\nu_{23}(b_2)$	620	**C═O bending**
ν_{23}(b)	526.3	C═O bending	$\nu_{19}(b_1)$	527	C═O bending
ν_{24}(b)	184.9	**ring C═O bending**	$\nu_{24}(b_2)$	215	**ring puckering**

[a] Bold typeface is used where our assignment differs significantly from the experimental one. In-phase and out-of-phase vibrations refer to the synchronization between the two CH_2 groups.

atoms are more involved in these vibrations. Nevertheless, in eight cases, the differences are substantial (see assignments marked in bold type in Table 3, ν_7, ν_{10}, ν_{11}, ν_{12}, ν_{17}, ν_{18}, ν_{22}, and ν_{24}). Most of these discrepancies occur in the low-frequency region where, due to the complexity of the vibrational modes, proper assignments are especially difficult. It is interesting to note, for instance, that the C═O bending has an unexpected noticeable weight on the lowest-frequency mode (ν_{24}). For the particular case of the ν_{17} and ν_{18} frequencies, the ring-stretching mode (ν_{18}) is assigned to a higher frequency than the CH_2 twisting in the experimental assignment[5] while the inverse order is found in the present ab initio calculation. Since these frequencies are very close (exp 5 cm^{-1}), it is difficult to ascertain the proper ordering.

As a rule of thumb, modes with (experimental) frequencies below 1139 cm^{-1} (that is, exactly the lower half of the modes) correspond to ring modes and/or C═O bendings (except for ν_{20}), while the higher upper half of the frequencies consists only of CH_2 modes and C═O stretchings. Finally, and as it is usually the case,[30] there is a substantial mismatch between the computed harmonic frequencies and the experimental ones for high (stretching) frequencies, with deviations of up to 200 cm^{-1} for the highest frequency mode (CH stretching), due to the increasing role of anharmonicities in that range. On the contrary, the accord is rather good for low frequencies, with some substantial deviations only in the (experimental) range of 700−960 cm^{-1}.

2. $[Li(EC)_n]^+$ (n = 1−4) Complexes. Regarding the effect of the ion on the solvent molecules vibrational frequencies and considering the results for the structure of the solvated complexes, it seems reasonable to expect that the strongest effects will be found for the dimer. While no experiments have been reported for this system, the computational estimation of the shift for this case should provide upper bounds of the liquid-phase ones. Indeed, we find that many of the frequencies of the single EC molecule coordinated to Li^+ are affected, with both substantial red- and blueshifts. In Table 4, the results for the dimer are compared with those previously discussed for the isolated EC molecule at the MP2/6-311++G(d,p) level. To ease the comparison with the vibrational frequencies of the single molecule, the notation ν_i is used for the 24 modes of EC (keeping the same numbering as before) and ω_i is used for the three modes where lithium is involved. The highest shifts occur in the ring-stretching and in the carbonyl-stretching modes; a blueshift of up to some 143 cm^{-1} for the ν_{18} ring mode and a redshift of up to 88 cm^{-1} for the important C═O mode (ν_3) are found.

TABLE 4: Harmonic Frequencies for EC and $[Li(EC)]^+$[a]

EC		$[Li(EC)]^+$		assignment	shift
ν_1(a)	3194.2	ν_1(a)	3227.0	out of phase CH_2 asym stretch	32.8
ν_2(a)	3109.7	ν_2(a)	3147.3	in phase CH_2 sym stretch	37.6
ν_3(a)	1898.8	ν_3(a)	1810.5	C═O stretching	−88.3
ν_4(a)	1546.8	ν_4(a)	1549.2	in phase CH_2 scissoring	2.4
ν_5(a)	1420.0	ν_5(a)	1425.8	out of phase CH_2 wagging	5.8
ν_6(a)	1271.5	ν_6(a)	1272.6	out of phase CH_2 twisting	1.1
ν_7(a)	1175.2	ν_7(a)	1172.0	out of phase CH_2 rocking	−3.2
ν_8(a)	1123.5	ν_8(a)	1146.6	os-ch sym stretch, ch-ch stretch	23.1
ν_9(a)	991.6	ν_9(a)	1012.1	ring breathing	20.5
ν_{10}(a)	895.3	ν_{10}(a)	941.4	ring breathing	46.1
ν_{11}(a)	719.6	ν_{11}(a)	786.7	ring stretching	67.1
		ω_1(a)	504.0	ring ox-Li^+ stretching	
ν_{12}(a)	227.2	ν_{12}(a)	184.4	out of plane ring bending	−42.8
ν_{13}(b)	3205.8	ν_{13}(b)	3239.8	in phase CH_2 asym stretch	34.0
ν_{14}(b)	3112.6	ν_{14}(b)	3149.3	out of phase CH_2 sym stretch	36.7
ν_{15}(b)	1539.4	ν_{15}(b)	1545.8	out of phase CH_2 scissoring	6.4
ν_{16}(b)	1420.8	ν_{16}(b)	1477.6	in phase CH_2 wagging	56.8
ν_{17}(b)	1267.9	$\tilde{\nu}_{18}$(b)[b]	1249.1	in phase CH_2 twisting	−18.8
ν_{18}(b)	1138.4	$\tilde{\nu}_{17}$(b)	1281.3	ring stretching	142.9
ν_{19}(b)	1079.2	ν_{19}(b)	1042.9	os-ch asym stretch	−37.2
ν_{20}(b)	919.0	ν_{20}(b)	904.0	in phase CH_2 rocking	−15.0
ν_{21}(b)	779.7	ν_{21}(b)	804.3	out of plane ring-C═O bending	24.6
ν_{22}(b)	673.4	ν_{22}(b)	697.5	in plane ring distortion	24.1
ν_{23}(b)	526.3	ν_{23}(b)	518.7	C═O bending	−7.6
ν_{24}(b)	184.9	ν_{24}(b)	228.4	ring C═O bending	43.5
		ω_2(b)	105.9	ring ox-Li^+ bending	
		ω_3(b)	58.8	cx-ox-Li^+ bending	

[a] Vibrational modes where lithium is involved are denoted by ω_i. [b] The tilde on two modes of the complex denotes the frequencies which exchange upon complexation (see text for explanation).

TABLE 5: Results of the Low-Level (MP2/6-31G) Vibrational Analysis for EC and Its Complexes with Lithium

	EC	$[Li(EC)]^+$	$[Li(EC)_2]^+$	$[Li(EC)_3]^+$	$[Li(EC)_4]^+$
ν_3(a)	1777.6	1733.8(−43.8)	1752.6(−25.0)	1765.2(−12.4)	1760.8(−16.8)
ν_4(a)	1584.8	1584.6(−0.2)	1585.1(+0.3)	1584.9(+0.1)	1584.4(−0.4)
ν_5(a)	1394.6	1394.1(−0.5)	1394.5(−0.1)	1394.5(−0.1)	1394.3(−0.3)
ν_6(a)	1259.4	1265.0(+5.6)	1264.2(+4.8)	1262.8(+3.4)	1261.6(+2.2)
ν_7(a)	1147.2	1139.4(−7.8)	1141.0(−6.2)	1142.2(−5.0)	1143.1(−4.1)
ν_8(a)	1020.3	1050.9(+30.6)	1042.5(+22.2)	1030.7(+10.4)	1024.4(+4.1)
ν_9(a)	946.0	978.9(+32.9)	974.8(+28.8)	965.6(+19.6)	957.5(+11.5)
ν_{10}(a)	795.0	835.0(+40.0)	837.6(+42.6)	830.7(+35.7)	824.2(+29.2)
ν_{11}(a)	680.6	760.6(+80.0)	752.2(+72.2)	723.4(+42.8)	705.8(+25.2)
ν_{12}(a)	162.0	82.8(−79.2)	102.0(−60.0)	123.2(−38.8)	138.2(−23.8)
ν_{13}(b)	1578.3	1575.3(−3.0)	1576.3(−2.0)	1576.7(−1.6)	1576.8(−1.5)
ν_{14}(b)	1402.4	1431.7(+29.3)	1424.2(+21.8)	1416.7(+14.3)	1412.0(+9.6)
ν_{15}(b)	1216.3	1214.5(−1.8)	1214.9(−1.5)	1215.1(−1.2)	1214.8(−1.5)
ν_{16}(b)	1025.6	1166.2(+140.6)	1139.5(+113.9)	1106.6(+81.0)	1087.0(+61.4)
ν_{17}(b)	974.1	944.3(−29.8)	956.4(−17.7)	967.2(−6.9)	973.9(−0.2)
ν_{18}(b)	886.4	874.1(−12.3)	876.0(−10.4)	878.1(−8.3)	880.0(−6.4)
ν_{19}(b)	694.3	721.6(+27.3)	718.2(+23.9)	711.5(+17.2)	708.3(+14.0)
ν_{20}(b)	663.3	701.9(+38.6)	694.7(+31.4)	685.2(+21.9)	678.8(+15.5)
ν_{21}(b)	487.9	486.6(−1.3)	486.5(−1.4)	485.0(−2.9)	502.3(+14.4)
ν_{22}(b)	176.5	226.5(+50.0)	218.1(+41.6)	209.5(+33.0)	202.5(+26.0)

Shifts relative to the single EC molecule are given in parentheses.

It is interesting to note that the substantial shift experienced by some modes may result in a reordering of frequencies. Two sorts of reordering are observed; the first concerns some frequencies within the same symmetry group. This is the case for the CH_2-twisting and the ring-stretching modes which, for the single EC molecule, are ν_{17}(b) and ν_{18}(b) respectively; it can be seen that this order is inverted in the lithium complex (see Table 4). A second type of reordering exists between frequencies corresponding to the two different symmetry groups. The two lowest-frequency modes constitute an interesting example: the harmonic value of the ring-bending mode ν_{12} (with A symmetry) is downshifted to 184 cm^{-1}, which is exactly the harmonic frequency of the unperturbed lowest-frequency mode ν_{24} (with B symmetry), which in turn is upshifted by the presence of the ion to 228 cm^{-1}, almost exactly the frequency of the unperturbed ν_{12}. Therefore, the two normal modes with the lowest frequencies are exchanged after EC coordinates the ion even if the same frequencies can still be found in the spectrum (such effects could be validated experimentally due to the different symmetry of both modes). A second example consists of the ν_{10} (A) mode (ring breathing), which experiences a blueshift, and the ν_{20} (B) (CH_2 twisting), which is shifted to lower frequencies, resulting in a crossing of their frequencies.

We have also analyzed the trends in the substantial ion-induced shifts upon addition of more solvent molecules. As mentioned above in section 3.1.2, it is to be expected that all shifts will diminish in absolute value since also the distortion of EC decreases with increasing solvation number. Starting from the optimized structures for the complexes that have been discussed in section 3.1.2, we have performed a vibrational analysis with the same model chemistry (MP2/6-31G) which provides useful insight into the trends. Table 5 contains the frequencies obtained for each complex together with the corresponding shifts relative to the single molecule (hydrogen-stretching modes are not included as this region is not relevant for solvation). Focusing on the dimer, the qualitative behavior of the shifts (see numbers in parentheses in the third column of Table 5) is very similar to that found at the MP2/6-311++G-(d,p) level (see last column of Table 4). Only in the case of very small shifts (<3 cm^{-1}), found for ν_4, ν_5, and ν_{15}, do the two calculations differ with respect to the direction of the shift.

Regarding the interpretation of Table 5, it should be noted that the number of normal modes increases rapidly with coordination number *n*. For every mode found in the single EC molecule, though, it is relatively easy to identify *n* (closely spaced) corresponding frequencies in the *n*-coordinated complex. Most of these frequencies are almost identical (differing by less than ∼1 cm^{-1}) so that just the average value is given. Since the amount of repulsion betwen original degenerate modes depends on the coupling between them, a few modes show a broader dispersion as *n* increases (see Table 6), in some cases with both red- and blueshifts (see first row, which corresponds to ν_3). It is to be expected that when such a substantial dispersion exists, the band splitting or at least a noticeable band broadening should be observed in liquid phase, as it is indeed the case for ν_3 and ν_{11} (see section 4.2).

TABLE 6: Low-Level (MP2/6-31G) Vibrational Analysis for EC Complexes: Details of the Modes That Show Non-Negligible Splitting of Frequencies[a]

	EC	$[Li(EC)_2]^+$	$[Li(EC)_3]^+$	$[Li(EC)_4]^+$
ν_3(a)	1777.6	1742.6(−35.0) 1762.5(−15.1)	1755.7(−21.9) 1755.8(−21.8) 1785.2(+7.6)	1753.4(−24.2) 1753.6(−24.0) 1753.6(−24.0) 1782.5(+4.9)
ν_{10}(a)	795.0	833.3(+38.3) 840.2(+45.2)	828.9(+33.9) 831.6(+36.6) 831.7(+36.7)	
ν_{11}(a)	680.6	721.8(+41.2) 782.6(+102.0)	714.1(+33.5) 727.9(+47.3) 728.1(+47.5)	702.7(+22.1) 706.0(+25.4) 707.3(+26.7) 707.3(+26.7)

[a] Shifts relative to the dimer frequencies are displayed in parentheses.

Turning to the behavior (of the averaged shifts) with varying number of molecules, we see as expected that the influence of lithium ion decreases upon increase of the coordination number. The two modes that are most affected in the dimer are the ring stretchings ν_{11} and ν_{18}. Figure 2 displays their shifts, together with those of the low-frequency ring bendings (ν_{12} and ν_{24}) and of the carbonyl bond stretching (ν_3), which is the mode most indicative of binding to the ion, as a function of the coordination number. In all cases, the shift estimated for the dimer is reduced by more than a 50% for the $n = 4$ complex. This is in agreement with the more modest shifts that will be shown to occur in the liquid (see below). The crossing of the ν_{12} and ν_{24} modes found for the dimer probably also disappear with increasing solvation number. It should be noted, though, that for the model chemistry

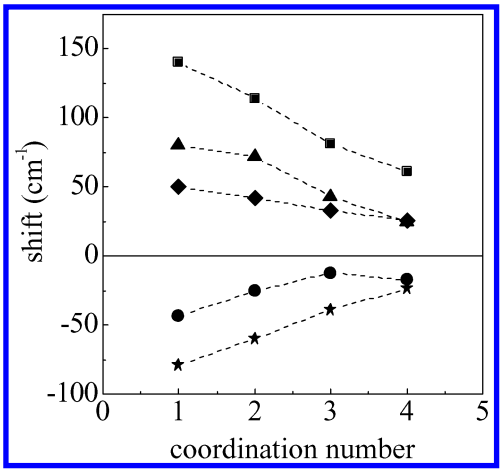

Figure 2. Computed shifts for lithium complexes as a function of coordination number. Five modes are shown: ν_3 (●), ν_{11} (▲), ν_{12} (★), ν_{18} (■), and ν_{24} (♦).

used here the single-molecule frequencies are more separated and no crossings occur. Nevertheless, value and sign of the shifts for the dimer are comparable to those obtained with the higher level of theory; since they are reduced by more than a 50% upon increasing the solvation number, it is likely that the mentioned crossing would disappear too.

C. Intramolecular Force Field. Finally, our ab initio calculations have been used to explore the full internal force field of the EC molecule, the rationale being that for the study of ion mobility in liquid EC it is important to handle properly the internal flexibility of the molecule. From the previous discussion of the spectrum, we see that four modes are found below ∼700 cm^{-1}, i.e., ∼3 k_BT (at 320 K, a typical temperature for liquid EC). Maybe even more important, the barriers for ring inversion are ∼2 k_BT (∼1.2 kcal mol^{-1}), and therefore it is reasonable to expect that some coupling may exist between ion mobility and ring dynamics in the solvation shell.

In this connection, it is to be noted that a popular force field like AMBER[32−34] performs poorly in reproducing the barriers to inversion and the absolute frequencies in the low-frequency range (see below). These considerations have motivated the development of a new force field from high-level ab initio calculations, tailored for EC. Particular attention has been payed to include effects beyond the simple adjustment of harmonic frequencies. In the most widely used procedure, an internal potential is constructed by grafting group (bond, etc.) contributions that have been fitted to represent a large body of molecules, usually only including harmonic terms (except for dihedrals). This method has the drawback that it can result in a rather bad accord for some frequencies. Table 7 contains the results for the AMBER force field as applied to EC; the six lowest harmonic frequencies (which are in principle the most relevant for liquid dynamics) are consistently too low by at least 20−40% compared with the ab initio or experimental values. The advantage in this sort of approach is that the functional form is standard and therefore implemented in most MD packages. If an accurate intramolecular potential is required, the most successful approach for molecules of a size similar to EC is to expand the internal potential in terms of normal modes.[30] While anharmonicity is treated more consistently, the drawback of this approach is that as the normal modes are computed numerically it is not evident how to implement it in a MD package.

Here we have devised a different approach to the problem of force-field development. We have tried to balance both approaches looking for both an easy implementation and a faithful representation of the actual anharmonic intramolecular potential. Starting from the optimized structure, we performed a rPES scan for all valence coordinates (stretchings, bendings, and dihedrals, including the ox-cx-os-os improper dihedral, which showed to be important in modeling low frequencies vibrations), with a

TABLE 7: Harmonic Frequencies Obtained with ab initio Calculations, Experimental Results, and Values Obtained with Classical Calculations Using Our New Force Field and the Amber Force Field[a]

	G98 (a)	exp (b)	new	diff$_a$	diff$_b$	amber	diff$_a$	diff$_b$
ν_1	3194.2	3000(w)	3225.0	30.8(1.0%)	225.0(7.5%)	2982.3	−211.9(−6.6%)	−17.7(−0.6%)
ν_2	3109.7	2925(w)	3143.3	33.6(1.1%)	218.3(7.5%)	2905.4	−204.3(−6.6%)	−19.6(−0.7%)
ν_3	1898.8	1868(vs)	2035.0	136.2(7.2%)	167.0(8.9%)	1623.4	−275.4(−14.5%)	−244.6(−13.1%)
ν_4	1546.8	1483(⊥)	1611.3	64.5(4.2%)	128.3(8.6%)	1567.7	20.9(1.3%)	84.7(5.7%)
ν_5	1420.0	1386(m)	1490.4	70.4(4.9%)	104.4(7.5%)	1448.4	28.4(2.0%)	62.4(4.5%)
ν_6	1271.5	1223(w)	1412.7	141.2(11.1%)	189.7(15.5%)	1401.9	130.4(10.3%)	178.9(14.6%)
ν_7	1175.2	1157(s)	1277.5	102.3(8.7%)	120.5(10.4%)	1174.8	−0.4(−0.0%)	17.8(1.5%)
ν_8	1123.5	1087(s)	1074.3	−49.2(−4.4%)	−12.7(−1.2%)	992.1	−131.4(−11.7%)	−94.9(−8.7%)
ν_9	991.6	881(w)	963.0	−28.6(−2.9%)	82.0(9.3%)	938.4	−53.2(−5.4%)	57.4(6.5%)
ν_{10}	895.3	715(m)	789.1	−106.2(−11.9%)	74.1(10.4%)	792.1	−103.2(−11.5%)	77.1(10.8%)
ν_{11}	719.6	660(?)B	669.1	−50.5(−7.0%)	9.1**(1.4%)**	544.4	−175.2(−24.3%)	−115.6**(−17.5%)**
ν_{12}	227.2	230[?]	223.3	−3.9(−1.7%)	−6.7**(−2.9%)**	175.9	−51.3(−22.6%)	−54.1**(−23.5%)**
ν_{13}	3205.8	3004(w)	3231.4	25.6(0.8%)	227.4(7.6%)	2988.8	−217.0(−6.8%)	−15.2(−0.5%)
ν_{14}	3112.6	2925(w)	3145.0	32.4(1.0%)	220.0(7.5%)	2910.1	−202.5(−6.5%)	−14.9(−0.5%)
ν_{15}	1539.4	1483(m)	1607.7	68.3(4.4%)	124.7(8.4%)	1522.5	−16.9(−1.1%)	39.5(2.7%)
ν_{16}	1420.8	1421(w)	1552.8	132.0(9.3%)	131.8(9.3%)	1464.3	43.5(3.1%)	43.3(3.0%)
ν_{17}	1267.9	1218[‖]	1296.7	28.8(2.27%)	78.7(6.5%)	1179.1	−88.8(−7.0%)	−38.9(−3.2%)
ν_{18}	1138.4	1125[w]	1116.1	−22.3(1.9%)	−8.9(−0.8%)	1044.4	−94.0(−8.3%)	−80.6(−7.2%)
ν_{19}	1079.2	960(m)	1061.5	−17.7(−1.6%)	101.5(10.6%)	986.2	−93.0(−8.6%)	26.2(2.7%)
ν_{20}	919.0	768(m)	896.9	−22.1(−2.4%)	128.9(16.8%)	861.1	−57.9(−6.3%)	93.1(12.1%)
ν_{21}	779.7	696(sh)	710.5	−69.2(−8.9%)	14.5**(2.1%)**	572.5	−207.2(−26.6%)	−123.5**(−17.7%)**
ν_{22}	673.4	620(?)B	660.4	−13.0(−1.9%)	40.4**(6.5%)**	494.8	−178.6(−26.5%)	−125.2**(−20.2%)**
ν_{23}	526.3	527(vw)	484.0	−42.3(−8.0%)	−43.0**(−8.2%)**	290.9	−235.4(−44.7%)	−236.1**(−44.8%)**
ν_{24}	184.9	215(m)B	185.9	1.0(0.5%)	−29.1**(−13.5%)**	169.7	−15.2(−8.2%)	−45.3**(−21.1%)**

[a] Key: The intensity of experimental peaks is given in brackets. [*] = solid-phase values; B = spectrum in benzene; w = weak; m = medium; s = strong; vs = very strong; ? = not reported in the literature; ⊥ (‖) = observed with perpendicular (parallel) polarized light.[5] Column diff$_a$ gives the difference between the values found with classical calculations and with the quantum chemical methods. The difference between classical and experimental values is shown in column diff$_b$. Bold typeface is used to point out the differences among classical simulations and experiment at low frequencies.

total of 19 coordinates scanned. At first sight, it could seem that we have scanned less coordinates than degrees of freedom, but due to the symmetry of the molecule, we have actually used more internal coordinates (39) than independent degrees of freedom (24, for example, the ch-os stretching appears twice with the same force constant). In Figure 3, we show some results: a bond (panel a), a bending angle (panel b), two dihedrals (panel c and d), and an improper dihedral angle (panel e). Fitting of these curves to suitable polynomials reveals that most of bond-distance rPES have a quartic behavior, while bending angles follow a third-order polynomial. For what concerns dihedral angles, we found that many of them show a double-well profile for the potential energy with an energy barrier of ~1.3 kcal mol^{-1}. The force-field parameters have been determined by imposing that every single rPES energy profile (computed with an in-house molecular mechanics code) matches the corresponding quantum chemically derived one over a whole range of values of the internal coordinate (not only at the minimum).

The following functional form has been used for the intramolecular potential (PES), which is the typical expansion in terms of valence coordinates plus anharmonic terms for stretchings (4th order) and bendings (3rd order)

$$V(r,\theta,\phi) = \sum_{\text{bonds}}[k_{r_2}(r-r_0)^2 + k_{r_3}(r-r_0)^3 + k_{r_4}(r-r_0)^4] + \sum_{\text{angles}}[k_{\theta_2}(\theta-\theta_0)^2 + k_{\theta_3}(\theta-\theta_0)^3] + \sum_{\text{dihedrals}}A_n[1+\cos(n\phi-\delta)] + \sum_{\text{improper}}k_{\phi_2}(\phi-\phi_0)^2 = V_{\text{stretchings}}(r) + V_{\text{bendings}}(\theta) + V_{\text{dihedrals}}(\phi) + V_{\text{improper}}(\phi) \quad (1)$$

where r, θ, and ϕ denote bond lengths, bending angles, and dihedral angles.

The initial approximation for the constants appearing in this expansion has been obtained from the ab initio rPES. For instance, the rPES for the ox-cx stretching has been fitted up to fourth order, and the corresponding constants have been introduced in formula 1. Though it is clear that rPES constants are in principle different from the corresponding internal coordinate contribution to the total PES, they constitute a convenient first guess. In an iterative procedure (in which classical rPES values are computed for each set of PES constants) all the parameters in the PES expansion have been scaled until the ratio of quantum and classical rPES values converged to a value better than 95% for *all* internal coordinates. It should be noted that an rPES profile does depend not only on its associated internal coordinate but also on the rest of internal coordinates (which are optimized at each point) so that the cross coupling between valence coordinates is implicitly taken into account. The final force field is reported in Tables 8, 9, and 10. Figure 3 shows the remarkable goodness of the fit by comparing the ab initio and classical rPES values for some selected examples. Panels a and c also display (dashed line) the potential profile computed with the AMBER force field for comparison. In the case of the bond stretching (panel a), we can appreciate that both the width and anharmonicity of the curve are better reproduced with the new parameters. Regarding the dihedral angles (panel d), the positions of the minima in the AMBER curve are displaced by ~±33° and the height of the barrier is underestimated with respect to the quantum chemically derived profile. Panel d displays one internal coordinate whose rPES value shows a discontinuity (also found for another coordinate as well). This feature can be interpreted as a sudden jump between stability basins along the minimum energy path represented by the rPES. It is remarkable that the

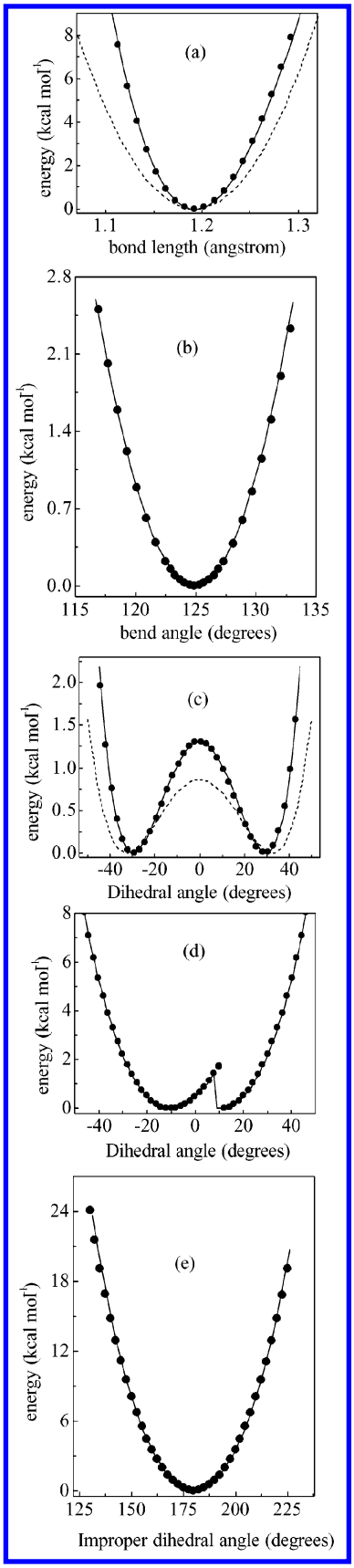

Figure 3. rPES curves for (a) ox-cx bond length, (b) ox-cx-os bending angle, (c) os-ch-ch-os dihedral angle, (d) os-cx-os-ch dihedral angle, and (e) ox-cx-os-os improper dihedral. The solid lines are obtained with a classical molecular mechanics program; dots are the results of the ab initio calculations performed with Gaussian 98; dashed lines in panels (a) and (c) are the profiles computed with the AMBER force field.

TABLE 8: Values of the Stretching Intramolecular Potential Constants and Comparison between Our New and the Amber Force Fields[a]

		new			amber
bond	r_0	k_{r_2}	k_{r_3}	k_{r_4}	k_{r_2}
ox-cx	1.193	973.54	−2385.37	−3627.64	540.4
cx-os	1.360	342.61	−931.29	1232.28	401.8
os-ch	1.430	317.74	−658.47	752.67	300.5
ch-ch	1.520	277.68	−552.40	736.85	307.6
ch-h	1.090	398.01	−812.09	1017.74	340.4

[a] Units: $[r_0]$ = Å, $[k_{r_2}]$ = kcal mol^{-1} Å^{-2}, $[k_{r_3}]$ = kcal mol^{-1} Å^{-3}, $[k_{r_4}]$ = kcal mol^{-1} Å^{-4}.

TABLE 9: Values for the Bending Intramolecular Potential Constants and Comparison between Our New and the Amber Force Field[a]

		new		amber
angle	θ_0	k_{θ_2}	k_{θ_3}	k_{θ_2}
ox-cx-os	124.970	71.43	−6.48	75.4
cx-os-ch	108.140	107.25	−3.33	62.0
ch-ch-os	102.050	119.09	−3.03	67.8
os-cx-os	110.200	139.74	−12.28	72.4
os-ch-h	108.600	65.09	−22.94	50.8
ch-ch-h	114.030	47.85	−16.44	46.5
h-ch-h	110.610	41.47	−21.59	39.3

[a] Units: $[\theta_0]$ = degrees, $[k_{\theta_2}]$ = kcal mol^{-6} rad^{-2}, $[k_{\theta_3}]$ = kcal mol^{-1} rad^{-3}.

TABLE 10: Values for the Constants Obtained for Dihedrals and Comparison between Our New and the Amber Force Field[a]

	new			amber		
dihedral	A_n	δ	n	A_n	δ	n
ox-cx-os-ch	1.400	180.0	1	1.400	180.0	1
ox-cx-os-ch	3.200	180.0	2	2.700	180.0	2
os-ch-ch-os	0.175	0.0	2	0.144	0.0	3
os-ch-ch-os	0.469	0.0	5	1.175	0.0	2
os-ch-ch-h	0.250	0.0	1	0.250	0.0	1
ch-ch-os-cx	0.800	180.0	1	0.800	180.0	1
ch-ch-os-cx	0.383	0.0	3	0.383	0.0	3
os-cx-os-ch	2.700	180.0	2	2.700	180.0	2
improper	ϕ_0	k_{ϕ_2}		ϕ_0	k_{ϕ_2}	
ox-cx-os-os	180.0	45.0d0				

[a] Units: $[\phi_0] = [\delta]$ = degrees, $[A_n]$ = kcal mol^{-1}, $[k_{\phi_2}]$ = kcal mol^{-1} rad^{-2}.

force field developed is able to reproduce even unusual aspects such as this one.

Finally, the harmonic part of this force field also provides satisfactory results in the low-frequency range, previously argued to be potentially important for liquid-state dynamics. The harmonic frequencies obtained for a single EC molecule are shown in Table 7. A *maximum* deviation of less than ∼10% is found for the six lowest frequencies (<700 cm^{-1}) when compared with the experimental values or with the ab initio harmonic frequencies. This good level of accord is maintained up to the highest frequencies, although in this range it is not manifestly superior to AMBER. Nevertheless, it is to be noted that for such an important mode like the C═O stretch (mode ν_3), the harmonic estimation with the present PES is larger than the experimental value (by ∼167 cm^{-1} while that of AMBER is *lower* by ∼244 cm^{-1}). It is obvious that when introducing anharmonic effects (contained in the present force field) the resulting frequency will be lower than the harmonic one, and therefore it is reasonable to expect that our PES value will come closer to the experimental value (a throughout study of the anharmonic frequencies is beyond the scope of this work and shall be addressed by the self-consistent methods of ref 30).

TABLE 11: Lennard-Jones Parameters and Charges for Intermolecular Interactions[35] [a]

atom type	σ_i (Å)	ϵ_i (kcal mol^{-1})	charge (e)
ox	2.96	0.210	−0.6452
cx	3.75	0.105	1.0996
os	3.00	0.170	−0.4684
ch	3.50	0.066	0.0330
h	2.50	0.030	0.1041
Li^+	1.46	0.191	1.0000

The values of atom−atom LJ constants are obtained with geometric mixing rules: $\sigma_{ij} = (\sigma_i\sigma_j)^{1/2}$ and $\epsilon_{ij} = (\epsilon_i\epsilon_j)^{1/2}$.

IV. Classical Computations

We have performed MD classical simulations with flexible molecules implementing our intramolecular force field. The following systems have been studied: one EC molecule; 215 EC molecules; 214 EC molecules + 1 lithium ion. All simulations were performed in the NVE ensemble with a time step of 0.2 fs. The reference temperature and density were set to 323.15 K and 1.3214 g cm^{-3}, respectively, in order to compare with previous works.[21,13]

Table 11 contains the parameters used for the intermolecular potential. Lennard-Jones parameters for EC are taken from Carlson et al.[35] (with geometric average combination rules). Partial charges on the atoms and LJ parameters for lithium ion are given by Soetens at al.[21] (fitted to the electrostatic potential-energy surface obtained by ab initio HF/6-31G** calculations). The Ewald sum was employed for the calculation of long-range interactions. Vibrational spectra were obtained by fast Fourier transform (FFT) of the dipole moment autocorrelation function[36,37,38,39,40,41] (see below).

A. Solvation Structure. In agreement with previous experimental[16] and theoretical studies,[13,15,21] our MD results for one lithium ion in liquid EC support the fact that four solvent molecules can be found within the first solvation shell. A more detailed study of the coordination structure around Li^+ shows its similarity with the ab initio calculation for the complex $[Li(EC)_4]^+$, with the carbonyl oxygen being the nearest site to the lithium ion (see panel a in Figure 4, which displays the atom−atom radial distribution functions for li-ox, li-cx, and li-os). The probability distribution of the li-os distance (panel b), restricted to molecules in the first coordination shell, clearly shows that one of the carbonate oxygens is nearer to the lithium ion than the other, the most probable distances being 3.8 and 4.0 Å, respectively (to be compared with 3.6 and 4.2 Å found in the 4-coordinated cluster, see section 3.1.2). The mean orientation of the EC molecules can be expressed by the angle between the molecular dipole moment (which, for symmetry reasons, is parallel to the ox-cx bond) and the vector pointing from the carbonyl oxygen to lithium. In panel c, it is shown that the most probable value for this angle is ∼162°. Therefore, the average $Li^+\cdots O{=}C$ angle in the liquid is larger than the optimized angle in the isolated dimer (see subsection 3.1.2). Finally, the dihedral angle formed by the four carbonyl oxygens around lithium is shown in panel d. It has two probability maxima at ∼68 and 111°. These values coincide with the ab initio results (∼68 and 112°). We can conclude that a tetrahedral-like structure is preserved in the liquid phase (the dihedral angle formed by the

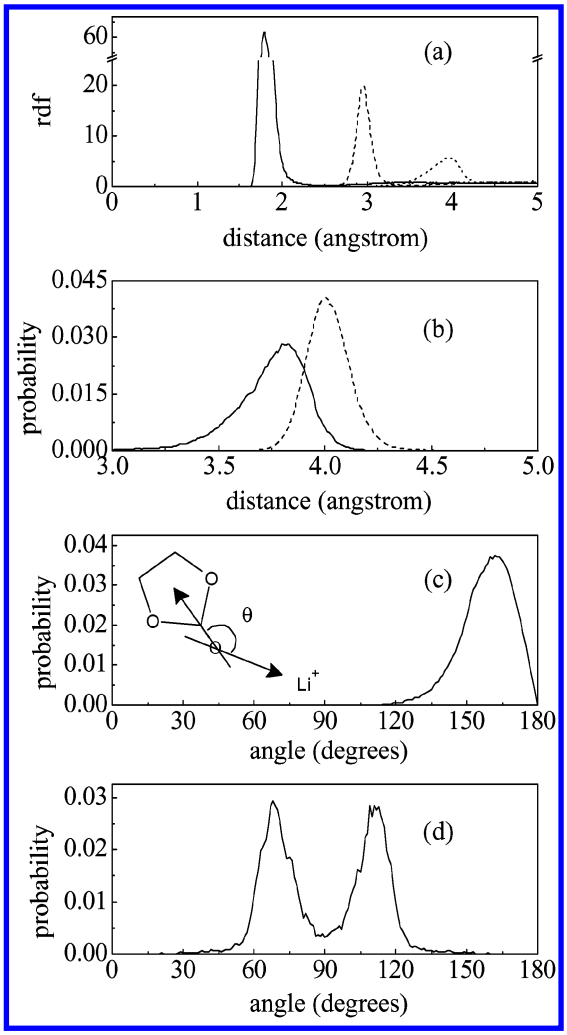

Figure 4. Results from MD simulation of the system EC−Li. (a) Atom−atom radial distribution function for li-ox (solid line), li-cx (dashed line), and li-os (dotted line); notice the broken scale on the *y* axis. (b) Probability distribution for the distance li-os$_1$ (solid line) and li-os$_2$ (dashed line), os$_1$ and os$_2$ being, respectively, the nearest and furthest carbonate oxygen in the same molecule. (c) Probability distribution for the angle θ between EC dipole moment and the vector li-ox (see inset). (d) Probability distribution for the dihedral angle formed by the 4 carbonyl oxygens nearest to lithium.

vertexes of a perfect tetrahedron is either 70.5 or 109.5°), with a slightly more parallel alignment between the EC dipole moment and the O···Li$^+$ vector in the liquid phase.

B. Vibrational Spectrum. Experiments so far mostly measured the ion-induced shifts in liquid EC. Here we will address this issue by means of MD simulations. It is important to emphasize that for this purpose the inclusion of anharmonicity is capital. The C═O stretch (which for the sake of the argument we can approximate as a local mode) can be used to illustrate this point. From first-order perturbation theory (*classical or quantal*), the induced shift on the simple vibration of a diatomic molecule is given by[42]

$$\delta\omega(t) = -\frac{3f}{\mu^2\omega_0^3}F_1(t) + \frac{1}{\mu\omega_0}F_2(t) \qquad (2)$$

where f is the coefficient of the cubic term in the gas-phase internal potential of the diatomic, μ is the reduced mass of the pair, and ω_0 is the gas-phase frequency. The following expansion in terms of the vibrational mode (Q) is used for the coupling (V) with the surrounding medium

$$V = \left[\frac{dV}{dQ}\right]_{Q=0} Q + \frac{1}{2}\left[\frac{d^2V}{dQ^2}\right]_{Q=0} Q^2 + ... + \equiv F_1 Q + F_2 Q^2 + ... \qquad (3)$$

It is often found[42−44] that only the first term in eq 2 contributes, so that the shift is mainly determined by the cubic anharmonicity (f, only in the case of CN$^-$ has the second term in formula 2 has been found to dominate).[45] Similar formulas, leading to the same conclusions regarding the importance of the cubic anharmonicity, can be derived in the general polyatomic case.[39] Therefore, if anharmonicity is not included (as it is the case in many conventional force fields), the computed shift is probably missing its main contribution. The fact that anharmonic terms are included in the intramolecular potential developed gives us confidence in the calculated shifts and it will be shown below that they are indeed consistent with both the trends found for the clusters and with the absolute shifts found in liquid-phase experiments.

Following Berens et al.,[36−38] the absorption line shape is given by

$$S(\omega) = (2\pi)^{-1}\int_{-\infty}^{\infty} dt\, \exp(-i\omega t)\langle \vec{M}(t)\cdot\vec{M}(0)\rangle \qquad (4)$$

where $\vec{M}$ denotes the total dipole moment. Consequently, the vibrational spectrum can be obtained from the FT of the total dipole moment time correlation function computed during a simulation, which is the simple approach that has been taken for the pure liquid. A central issue is how the ion affects the vibrational frequencies of the first-shell solvent molecules. To this end, the dipole moments of these molecules were stored separately during the simulation of an ion immersed in a EC liquid, extracting the ion-perturbed spectrum from this time series. Since solvent exchanges take place between first and second ionic solvation shells, we were able to follow a single molecule residing in the first shell only up to a maximum of ∼48 ps, this being the largest residence time observed in a simulation of 200 ps. The shortness of this time series results in a non-negligible degree of noise so that a filter is required. To illustrate the effect of this smoothing, the raw spectrum and the filtered one of the carbonyl-stretching mode are shown in Figure 6.

The whole vibrational spectrum of the neat liquid is compared with that of a single EC molecule in Figure 5. They are displayed on different panels due to their overall similarity; the peak positions are coincident, and the only difference is the usual broadening of the bands in the liquid state. The coincidence of vibrational frequencies can be explained by the weak interactions among EC molecules in the condensed phase. Indeed, by means of ab initio calculations, Li et al.[12] found that there is no strong attractive interaction between EC molecules.

From our ab initio calculation of the harmonic spectrum of EC and of the complexes [Li(EC)$_n$]$^+$, it is clear that all modes involving the ring and the carbonyl oxygen should be affected by solvation. The shifts reported in Table 3 can be considered as an upper bound to those in the liquid phase since, as discussed in section 3 and 3.2.2, the interaction among Li$^+$ and EC is strongest for the dimer. Nevertheless, they are indicative of the changes that might be found upon solvation of the lithium ion; the most important shifts (higher than 30 cm^{-1} in the dimer) are calculated to occur for ν_3, ν_{10}, ν_{11}, ν_{12}, ν_{16}, ν_{18}, ν_{19}, and ν_{24}. Indeed, liquid-phase experiments have focused on ν_3, ν_{10}, ν_{11}, ν_{16}, and ν_{19}. In Figure 7, we show the comparison between the

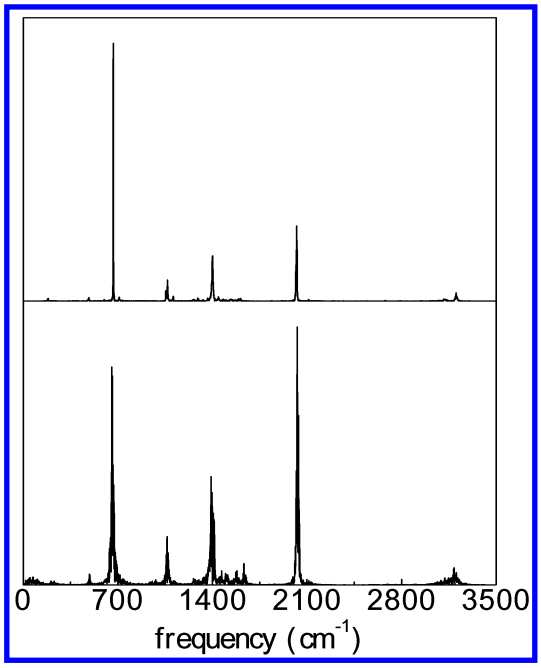

Figure 5. Simulated spectra for EC for a single molecule (upper panel) and for 215 molecules in the condensed phase (lower panel).

MD spectrum for the pure liquid and the one for the first-shell molecules. Five important regions, corresponding to the above cited bands, are enlarged in order to better discern the shifts induced by ion coordination in the liquid phase, which will be addressed in turn.

Experimentally, it has not been possible to determine if a shift exists for the C═O stretch mode (ν_3) due to the overlap with Fermi resonances.[31] Only a broadening of the band is clearly found to be an effect of the lithium ion. Hyodo et al.[16] extracted a little redshift, pointing out that this mode is unsuitable for the investigation of ion−solvent interactions; Wang et al.[19] reported a change in the carbonyl stretching but they did not quantify it; Klassen et al.[11] observed a change of the band shape in their Raman spectra as lithium perchlorate concentration was increased. Moreover, for the system PC−lithium (very similar to EC−lithium), Battisti et al.[46] observed a broadening of 27 cm^{-1} in the full width at half maximum of this spectral line at high ionic concentrations. These results are consistent with what was found in section 3.2.2 for the 4-coordinated complex: both red- and (smaller) blueshifts exist for the carbonyl stretching, resulting in an average small resdshift of ∼17 cm^{-1}. The second panel of Figure 7 shows the C═O stretching band both for neat EC and for those molecules within the first solvation shell, as obtained from the MD simulations of the liquid. A redshift of ∼20 cm^{-1} is observed (much lower than the 88 cm^{-1} predicted for the dimer in the higher level calculations). This shift is comparable both with the cited line broadening observed experimentally[11,46] and with the result of ab initio calculation on the 4-coordinated complex. Therefore, the present results support the notion that the observed broadening is mainly due to an ion-induced redshift of the molecules within the first solvation shell.

Some frequencies are missing in the simulated spectrum, usually corresponding to the ones with lower intensity in the experiment. Although in a harmonic analysis of a single molecule all frequencies are obtained, the liquid-phase spectrum is computed from the total dipole moment time correlation function, and therefore, the change of dipole moment and the signal−noise ratio determines which modes can be detected. In particular, the ring breathing mode at ∼900 cm^{-1} (ν_{10}) cannot be discerned. Experimentally, this mode seems to split when EC coordinates lithium, an effect that depends on lithium concentration.[16] A similar case is that of the ν_{18} band, which is also missing. This is the mode which, in our quantum chemical calculations, undergoes the highest blueshift. In line with the initial considerations, no experimental observations have been reported for this mode as its intensity is very weak (see Table 7).

The ring-stretching mode (ν_{11}) is shown in the third panel. Hyodo et al.[16] found that this band shows a typical shoulder or splitting of ∼15 cm^{-1} upon solvation of the electrolyte (though they attributed the vibration to the carbonyl-bending mode). This measured splitting clearly appears in our spectrum. Similar to the behavior found for ν_3, the ab initio calculated blueshift for this mode in the dimer is 67 cm^{-1}, while in the MD simulation we obtain a smaller blueshift of ∼28 cm^{-1}, which compares very well with the experiment. It is to be noted that this is not a simple shift of the band for those molecules in the first shell, as it occurred for the carbonyl-stretching mode. Here, the first-

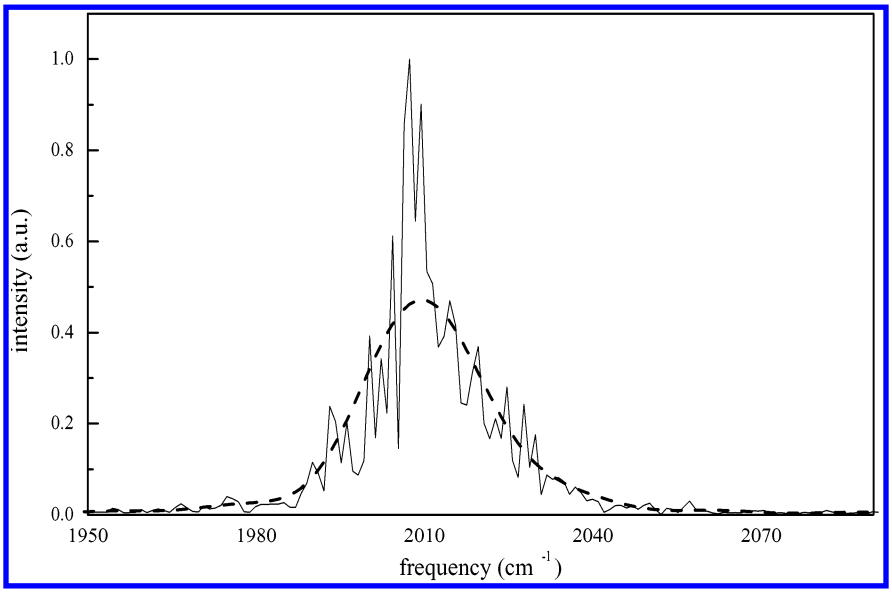

Figure 6. Original (noisy) spectrum (solid line) and filtered spectrum (dashed line) of EC as used for the FFT of the dipole moment correlation function.

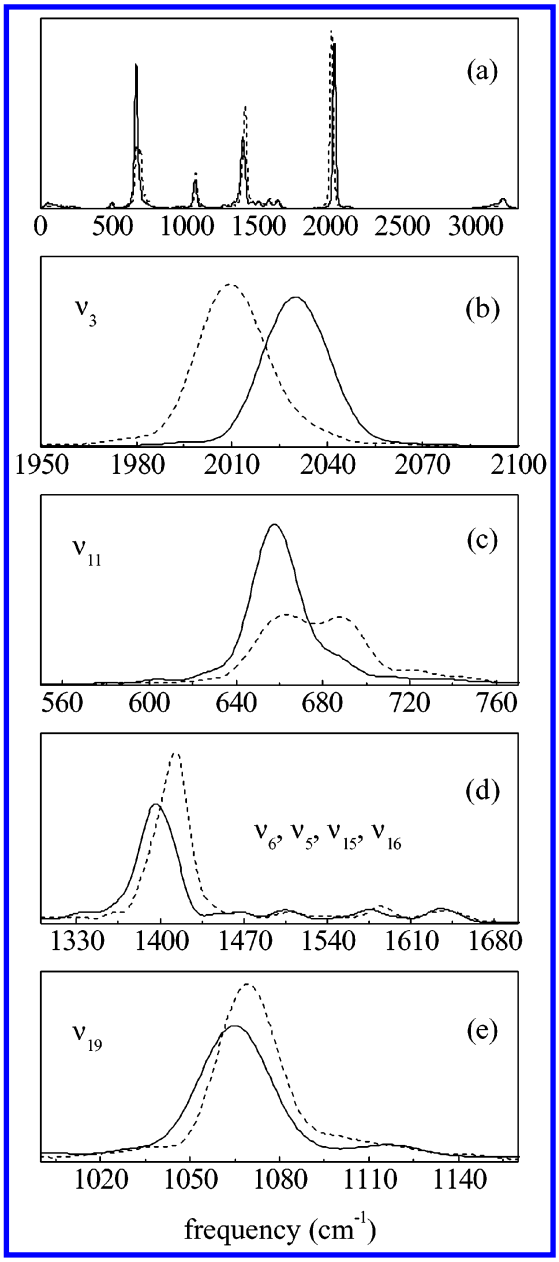

Figure 7. Comparison of the simulated spectra of EC (solid line) and EC−Li^+ (dashed line). The whole spectra are shown in panel a. Subsets of spectral regions as discussed in the text are shown in the lower panels.

shell molecules contribute equally to both peaks. This suggests that, while the average structure is tetrahedral, interconversions between metastable substructures in the first shell might take place on a shorter time scale.

Experimentally, the hydrogen−carbon stretching and bending modes (ν_{16}, ν_{15}, ν_6, and ν_5) are largely unaffected by the coordination to the ion.[11] This is also the basic conclusion of this work; in the ab initio calculations, we find small shifts (see section 3.2.2 and Tables 4 and 5), and in our MD simulations, we find only small blueshifts of these bands as well. Panel d of Figure 7 displays this for the CH_2 twisting (ν_6), for which the largest shift ($\sim$15 cm^{-1}) is found. The other bands are shifted by only $\sim$9 (ν_{16}) and 5 cm^{-1} (ν_{15} and ν_5), respectively.

Finally, Klassen et al.[11] pointed out that the ring C−O stretching vibrations (ν_{19}) are affected by the presence of lithium ions, although quantitative estimations were not given. For this vibration, we obtain from the quantum chemical calculation a redshift of 37 cm^{-1} (see Table 4), while the simulated shift is $\sim$5 cm^{-1} for the ν_{19} band (panel e).

V. Conclusions

Structural and dynamical properties of EC in the gas and liquid phases have been studied. High level ab initio calculations support the notion of a C_2 equilibrium symmetry for this molecule. This nonplanar structure persists upon solvation of the lithium ion, with a slight tendency to planarity for small solvation numbers. The barriers to internal motion are in all cases in the thermal range, which suggests that a non-neglibigle coupling with first-shell dynamics might exist. A new assignment of vibrational modes is proposed that takes into account the nonplanarity in contrast to previous assignments. Lithium ion coordination induces substantial red and blue vibrational frequency shifts in the gas phase, resulting in a reordering of modes in a few cases. To handle properly the low-energy vibrations at typical liquid state conditions, an intramolecular force field has been specifically developed for EC. The methodology devised for this purpose is aimed at faithfully reproducing the rPES for all valence coordinates, a goal that has been achieved to a considerable degree. This force field has allowed the computation of the vibrational spectrum via classical simulation for the condensed phase. Both in the case of the neat liquid and in the close vicinity of the ion, the results reproduce satisfactorily the experimental measurements. Lithium coordination induces shifts mainly in the ring motions and in the carbonyl-stretching bands of the four EC molecules lying in the first coordination shell. Most of the vibrations are shifted to higher wavenumbers except for the carbonyl-stretching mode, which exibits a redshift typically found in the bond containing an oxygen atom directly coordinating to a metal cation. The broadening of the band observed experimentally seems thus related to this shift and supports the notion that the carbonyl groups are oriented toward the ion.

Acknowledgment. This work was supported by the EC TMR network HPRN-CT-2000-19 (“Solvation Dynamics and Ionic Mobility in Conventional and Polymer Solvents”) and MCYT project BFM2001-2077. We thank E.L. Sibert for useful comments.

References and Notes

(1) Song, J. Y.; Wang, Y. Y.; Wan, C. C. *J. Power Sources* **1999**, *77*, 183.
(2) Sekhon, S. S.; Deepa and Agnihotry, S. A. *Solid State Ionics* **2000** *136*−*137*, 1189.
(3) Angell, C. L. *Trans. Faraday Soc.* **1956**, *52*, 1178.
(4) Wang, J.; Britt, C. O.; Boggs, J. E. *J. Am. Chem. Soc.* **1965**, *87*, 4950.
(5) Fortunato, B.; Mirone, P.; Fini, G. *Spectrochim. Acta* **1971**, *27A*, 1917.
(6) Alonso, J. L.; Cervellati, R.; Esposti, A. D.; Lister, D. G.; Palmieri, P. *J. Chem. Soc., Faraday Trans. 2* **1986**, *82*, 337.
(7) Alonso, J. L.; Cervellati, R.; Esposti, A. D.; Lister, D. G.; Palmieri, P. *J. Chem. Soc., Faraday Trans. 2* **1986**, *82*, 357.
(8) Matias, P. M.; Jeffrey, G. A.; Wingert, L. M.; Ruble, J. R. *THEOCHEM* **1989**, *184*, 247.
(9) Esposti, A. D.; Lister, D. G.; Palmieri, P. *J. Mol. Struct.* **1990**, *223*, 325.
(10) Blint, R. *J. Electrochem. Soc.* **1995**, *142*, 696.
(11) Klassen, B.; Aroca, R.; Nazri, M.; Nazri, G. A. *J. Phys. Chem. B* **1998**, *102*, 4795.
(12) Li, T.; Balbuena, P. B. *J. Electrochem. Soc.* **1999**, *146* (10), 3613.
(13) Soetens, J. C.; Millot, C.; Maigret, B.; Bakó, *J. Mol. Liq.* **2001**, *92*, 201.
(14) Wang, Y.; Balbuena, P. B. *J. Phys. Chem. A* **2001**, *105*, 9972.
(15) Wang, Y.; Nakamura, S.; Ue, M.; Balbuena, P. B. *J. Am. Chem. Soc.* **2001**, *123*, 11708.

(16) Hyodo, S. A.; Okabayashi, K. *Electrochim. Acta* **1989**, *34* (11), 1551.
(17) Cazzanelli, E.; Croce, F.; Appetecchi, G. B.; Benevelli, F.; Mustarelli, P. *J. Chem. Phys.* **1997**, *15*, 5740.
(18) Castriota, M.; Cazzanelli, E.; Nicotera, I.; Coppola, L.; Oliviero, C.; Ranieri, G. A. *J. Chem. Phys*. **2003**, *118*, 5537.
(19) Wang, Z.; Huang, B.; Huang, H.; Xue, R.; Chen, L.; Wang, F. *J. Electrochem. Soc*. **1996**, *143* (5), 1510.
(20) Wang, Z.; Huang, B.; Xue, R.; Chen, L.; Huang, X. *J. Electrochem. Soc*. **1998**, *145* (10), 3346.
(21) Soetens, J. C.; Millot, C.; Maigret, B. *J. Phys. Chem. A* **1998**, *102* (7), 1055.
(22) Frisch, M. J.; Trucks, G. W.; Schlegel, H. B.; Scuseria, G. E.; Robb, M. A.; Cheeseman, J. R.; Zakrzewski, V. G.; Montgomery, J. A., Jr.; Stratmann, R. E.; Burant, J. C.; Dapprich, S.; Millam, J. M.; Daniels, A. D.; Kudin, K. N.; Strain, M. C.; Farkas, O.; Tomasi, J.; Barone, V.; Cossi, M.; Cammi, R.; Mennucci, B.; Pomelli, C.; Adamo, C.; Clifford, S.; Ochterski, J.; Petersson, G. A.; Ayala, P. Y.; Cui, Q.; Morokuma, K.; Malick, D. K.; Rabuck, A. D.; Raghavachari, K.; Foresman, J. B.; Cioslowski, J.; Ortiz, J. V.; Stefanov, B. B.; Liu, G.; Liashenko, A.; Piskorz, P.; Komaromi, I.; Gomperts, R.; Martin, R. L.; Fox, D. J.; Keith, T.; Al-Laham, M. A.; Peng, C. Y.; Nanayakkara, A.; Gonzalez, C.; Challacombe, M.; Gill, P. M. W.; Johnson, B. G.; Chen, W.; Wong, M. W.; Andres, J. L.; Head-Gordon, M.; Replogle, E. S.; Pople, J. A. *Gaussian 98*, revision A.11.2; Gaussian, Inc.: Pittsburgh, PA, 1998.
(23) Frisch, M. J.; Pople, J. A.; Binkley, J. S. *J. Chem. Phys*. **1984**, *80*, 3265.
(24) DL_POLY is a package of molecular simulation routines written by W. Smith and T. R. Forester, copyright The Council For The Central Laboratory Of The Research Council, Daresbury Laboratory at Daresbury, Nr. Warrington 1996.
(25) http://www.dl.ac.uk/TCSC/Software/DL_POLY/main.html
(26) http://www.originlab.com
(27) Cremer, D.; Pople, J. A. *J. Am. Chem. Soc.* **1975**, *97*, 1354.
(28) Schlegel, H. B. *J. Comput. Chem*. **1982**, *3* (2), 214.
(29) Peng, C.; Ayala, P. Y.; Schlegel, H. B.; Frisch, M. J. *J. Comput. Chem*. **1996**, *17* (1), 49.
(30) Chaban, G. M.; Jung, J. O.; Gerber, R. B. *J. Phys. Chem. A* **2000**, *104*, 10035.
(31) Wilson, E. B.; Decius, J. C.; Cross, P. C. *Molecular Vibrations*; Dover Publications Inc.: New York, 1980.
(32) Weiner, S. J.; Kollman, P. A.; Nguyen, D. T.; Case, D. A. *J. Comput. Chem*. **1986**, *7*, 230.
(33) Cornell, W. D.; Cieplak, P.; Bayly, C. I.; Gould, I. R.; Merz, K. M.; Ferguson, D. M.; Spellmeyer, D. C.; Fox, T.; Caldwell, J. W.; Kollman, P. A. *J. Am. Chem. Soc.* **1995**, *117*, 5179.
(34) http://www.amber.ucsf.edu/amber/dbase.html
(35) Carlson, H. A.; Nguyen, T. B.; Orozco, M.; Jorgenden, W. L. *J. Comput. Chem*. **1993**, *14* (10), 1240.
(36) Berens, P. H.; Wilson, K. R. *J. Chem. Phys*. **1981** 74 (9), 4872.
(37) Berens, P. H.; White, S. R.; Wilson, K. R. *J. Chem. Phys*. **1981** 75 (2), 515.
(38) Berens, P. H.; Mackay, D. H. J.; White, G. M.; Wilson, K. R. *J. Chem. Phys*. **1983**, *79* (5), 2375.
(39) Katō, T.; Machida, K.; Oobatake, M.; Hayashi, S. *J. Chem. Phys*. **1990**, *93* (6), 3970.
(40) Nakagawa, T.; Umemura, J.; Hayashi, S.; Oobatake, M.; Miwa, Y.; Machida, K. *Mol. Phys*. **1996**, *88* (6), 1635.
(41) Henssge, E.; Dumont, D.; Fischer, D.; Bougeard, D. *J. Mol. Struct*. **1999**, *482*−*483*, 491.
(42) Oxtoby, D. W.; Levesque, D.; Weiss, J.-J. *J. Chem. Phys*. **1978**, *68*, 5528.
(43) Laaksonen, A.; Westlund, P.-O. *Mol. Phys*. **1991**, *73*, 663.
(44) Rey, R.; Moller, K. B.; Hynes, J. T. *J. Phys. Chem. A* **2002**, *106*, 11993.
(45) Rey, R.; Hynes, J. T., *J. Chem. Phys*. **1998**, *108*, 142.
(46) Battisti, D.; Nazri, G. A.; Klassen, B.; Aroca, R. *J. Phys. Chem.* **1993**, *97*, 5826.